Chapter 3
The Comparison of Observational and Simulation Data

Cathie J. Clarke

Before we describe the results of star formation simulations in detail, we need to consider how, in principle, one should decide whether the output of a simulation is a good match to reality. This issue is not entirely straightforward given the complex morphology and hierarchical nature of observed molecular clouds (and also of numerical simulations). For example, the fact that simulations generally produce filamentary and highly structured clouds with a mixture of clustered and more distributed star formation is at first sight encouraging, because these are broadly properties shared by observed clouds (Men'shchikov et al. 2010; Peretto et al. 2012; Schneider et al. 2012). One however needs a more refined measure of whether simulations and observations are indeed quantitatively consistent. We therefore conduct a brief survey of statistical descriptors that have been applied to simulations and observations. We follow this by applying some of these methods to the simplest class of star cluster formation simulations (termed 'vanilla' calculations in these chapters) which contain only the three most basic physical ingredients: gas pressure, turbulence and gravity.

3.1 The Characterisation of Observational and Simulated Data

3.1.1 Characterising Gaseous Structures

There are many alternative descriptors of the wealth of structures found in the density and velocity fields of molecular clouds (see Blitz and Stark 1986 for early analyses of the hierarchical nature of the interstellar medium). For example, Padoan et al. (2003) analysed ^{13}CO emission maps of Taurus and Perseus by computing *structure functions* as a function of r (i.e. expectation values of the pth power of the difference

C.J. Clarke (✉)
Institute for Astronomy, University of Cambridge, Cambridge, UK
e-mail: cclarke@ast.cam.ac.uk

C.P.M. Bell et al. (eds.), *Dynamics of Young Star Clusters and Associations*,
Saas-Fee Advanced Course 42, DOI 10.1007/978-3-662-47290-3_3

in intensity between points in the map separated by distance r): the power-law dependence of the structure function on r indicates the scale-free nature of much of the structure within molecular clouds. Padoan et al. (2003) attempted to compare these results with the predictions of various turbulence models for the form of the structure function for velocity. The relationship between structure functions for intensity and those for velocity (as derived in the case of supersonic turbulence; Boldyrev 2002) is however unclear.

A more intuitive method of analysing molecular cloud structures is via the use of *dendrograms*. These can be visualised by considering a dataset (e.g. integrated intensity as a function of two-dimensional position) as a topographical surface which one then 'thresholds' at various levels, identifying the distinct peaks above each threshold and tracing how these merge as the threshold level is reduced. (A good analogy here is how the distribution of 'islands' changes as the water level around a flooded mountain range is reduced.) The structure can then be depicted in terms of a network of branches whose geometry reflects the hierarchical organisation of the medium (see Fig. 3.1). Rosolowsky et al. (2008) applied such an analysis to the L1448 region of the Perseus molecular cloud and compared this with simulations of MHD turbulence by Padoan et al. (2006); they noted that dendrogram analysis can in some cases identify discrepancies between simulations and observations that are not discernible through analysis of the power spectrum (the power spectrum simply counts entities on different scales without directly assessing the spatial relationship between structures on different scales).

By far the most widely used algorithms for analysing the structure of molecular clouds are those of a 'friend of friends' type, such as the CLUMPFIND algorithm (Williams et al. 1994) which identifies peaks and then works downwards in intensity, assigning neighbouring regions to their local intensity peak and otherwise creating a new clump which is treated in the same way. Such an approach can be used to identify distinct clumps either in positional data or else, in the case of line emission maps, in

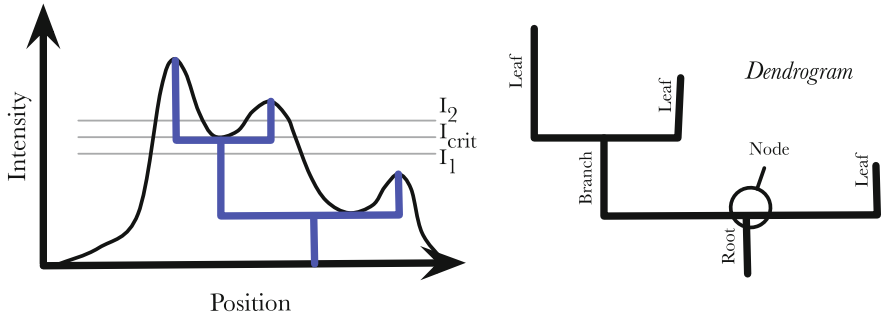

Fig. 3.1 A schematic depiction of how dendrogram analysis leads to the rendering of intensity positional data in terms of a root-branch-leaf structure. The *left panel* shows a one-dimensional emission profile with three distinct local maxima. The dendrogram of the region is illustrated in blue and shown in the *right panel* where the components of the dendrogram are labelled. Figure from Rosolowsky et al. (2008)

datacubes in joint positional and velocity space. Once such clumps have been identified, one can readily construct their mass spectrum (commonly termed the CMF: clump mass function) and compare with the corresponding quantity derived from simulations (see Klessen and Burkert 2000; Smith et al. 2008 for the application of such analyses to datacubes generated by SPH simulations). The extraction of a clump mass spectrum from either observations or simulations is however a non-unique procedure. As emphasised in their paper 'The perils of CLUMPFIND...', Pineda et al. (2009) conclude that the derived clump spectrum is highly dependent on the observational resolution and that, in particular, kinematic data is required to disentangle structures that are blended along the line of sight. In other studies, independent analyses of millimetre maps of ρ Ophiuchus (Motte et al. 1998; Johnstone et al. 2000) agree about the mass spectrum of the derived clumps but disagree about the masses and locations of individual clumps. Moreover, Smith et al. (2008) found (through applying the CLUMPFIND algorithm to simulation data) that the overall shape of the derived clump mass spectrum was fairly insensitive to the CLUMPFIND parameters employed but that the location of apparent breakpoints was rather strongly dependent on these algorithmic parameters. This result underlines the fact that such a method can only be used to compare observations and simulations if the algorithmic details, and the resolution, are well matched. It also raises obvious questions about the *physical* significance (if any) of such breakpoints in the derived CMF.

3.1.2 Characterising Stellar Distributions

We now turn to the issue of characterising stellar spatial distributions. One of the first measures to be applied to large-scale distributions of stellar positions was the Mean Surface Density of Companions (MSDC, Larson 1995; Simon 1997; Bate et al. 1998). This measure is computed by counting all the stars within an annulus of given radius (r) centred on each star, dividing by the area of the annulus, repeating this procedure with the annulus centred at every star in the region, and then averaging to obtain the mean surface density at that separation. The MSDC is thus closely related to the two-point correlation function which instead subtracts off the large-scale mean surface density: although appropriate to cosmological studies (where the distribution of galaxies is expected to be uniform on the largest scales) this is not useful in star-forming regions which are generally inhomogeneous on scales extending up to the size of the entire region analysed.

Analyses of nearby star-forming regions revealed a double power-law structure in the MSDC: the inner power-law is readily identified with size scales where stars have one companion on average—in other words it corresponds to the distribution of nearest neighbour (in reality bound—i.e. binary star—companion) distances. Since the binary separation distribution is rather flat in log separation, this translates into a MSDC of slope -2. At larger separations it transitions to a shallower slope which Larson (1995) interpreted as evidence of fractal clustering on larger scales (i.e. clustering with no characteristic size scale but a self-similar relationship between surface

density and size). Bate et al. (1998) however argued that this interpretation was not unique and that global density gradients or non-fractal sub-clustering would also be consistent with the data over the limited dynamic range of size scales (2–3 orders of magnitude) between the binary regime and the total size of star forming regions.

Alternative measures of stellar distributions can be derived from the Minimum Spanning Tree (MST), which is the unique connection of points in a dataset so as to minimise the total length without involving any closed loops. Cartwright and Whitworth (2004) proposed a single number (the Cartwright Q parameter) that can be used to classify the nature of stellar distributions. Q is defined as the ratio of the value of $\bar{m}$ (the mean edge length normalised to the mean value for N random points in the area) to $\bar{s}$ (the 'normalised correlation length', i.e. mean separation divided by the cluster radius). The important distinction is that whereas the mean edge length refers to the mean separation of closest neighbours (i.e. those directly linked by the MST), the mean separation is the mean (over all stars) of the distance to *all the other stars* in the cluster.

We can start to understand how the Q parameter is able to distinguish qualitatively different stellar distributions by first considering a uniform distribution of points—empirically this yields a particular Q value ($\sim$0.7). Now we consider two different ways of driving the distribution away from the uniform: in both cases we move stars around so that there is now a range of densities, but whereas in one case the high-density regions are co-located (which we call the centrally concentrated case) in the other the islands of high-density are spatially dispersed (which we call the fractal case). As one moves away from the uniform distribution, both $\bar{m}$ and $\bar{s}$ are reduced as stars are brought closer together. However, the reduction in $\bar{s}$ is relatively small in the fractal case because when stars are moved to isolated high-density peaks, this affects the mean separation of relatively few stars. Consequently, Q falls as one proceeds from a uniform distribution to fractal distributions with decreasing fractal dimension (i.e. distributions that are more clumped); conversely Q increases as one proceeds from uniform distributions to distributions that are increasingly centrally concentrated. In general, real stellar distributions are neither necessarily centrally concentrated nor strictly fractal so the real utility of the Q parameter is that it provides a ready way to distinguish distributions in which high-density regions are co-located from those in which they are spatially dispersed. As such it is a useful tool when one compares the outcome of simulations with real observational data (see e.g. Schmeja et al. 2008).

Another use of the MST is that it can provide a simple empirical definition of a 'cluster': one can specify a 'cut-length' and sever all branches of the tree that exceed this length, thereby dividing a distribution of points into a set of distinct 'clusters'. Naturally, the numbers and identities of such 'clusters' are highly sensitive to the cut-length employed (see Fig. 3.2). Although the definition of clusters is thus arbitrary (and certainly does not correspond to entities that are necessarily gravitationally bound) it at least provides a consistent way to compare a simulation set with an observational dataset (provided, of course, that both datasets are analysed with the same cut-length; see Maschberger et al. 2010 for an analysis of the 'clustering' within the simulations of Bonnell et al. 2003, 2008 using this method).

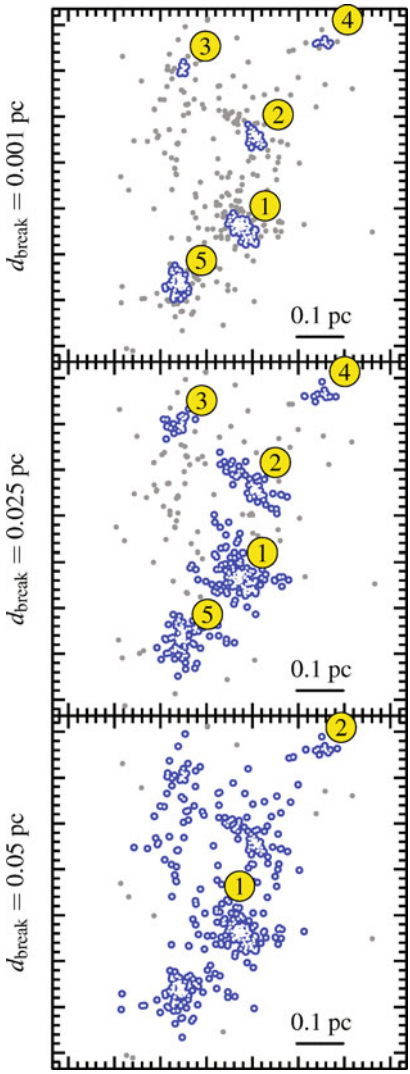

Fig. 3.2 Illustration of the use of the minimum spanning tree in identifying 'clusters' (*numbered circles*) in the simulations of Bonnell et al. (2008). The three panels show how the 'clusters' identified depend on the value of the cut-length parameter $d_{\rm break}$ adopted (0.001, 0.025 and 0.05 from *top* to *bottom* respectively). Figure from Maschberger et al. (2010)

One of the most widely used applications of the MST is to characterise *mass segregation* within observational and simulation datasets. There is considerable interest in whether massive stars are preferentially located in dense regions and whether this is a consequence of two-body relaxation or instead reflects stellar birth sites. In the case of spherically symmetric clusters, mass segregation may be evaluated by comparing the radial distributions of stars as a function of mass (e.g. Bate 2009; Moeckel and Bonnell 2009). Such an approach is obviously not appropriate in the commonly encountered situation where stellar distributions lack any clear symmetry and this is where MST based techniques offer a clear advantage: Allison et al. (2009) proposed

a method in which the mean edge length of the MST constructed from the i most massive stars is calculated and then compared with the corresponding quantity constructed from a MST based on random samples of i stars. The ratio of these quantities Λ is a measure of whether the i most massive stars are similarly distributed to the general population: its particular advantage is that it is self-calibrating because when one computes the mean edge length of i random stars through repeated sampling one obtains also the standard deviation of that quantity and thus can readily assess whether the value for the i most massive stars is significantly different. Results however need to be interpreted with care because the mean edge length is highly sensitive to the maximum edge length in the distribution. For example, in Taurus the mean edge length for massive stars is large because of a few massive stars lying at large distances from the remainder; this can produce an apparent signature of 'inverse mass segregation' even though the majority of massive stars in Taurus are actually more closely associated with each other than is the case for 'typical' (lower mass) stars in the region (Parker et al. 2011). The interpretation of the Λ statistic is thus improved if one also compares quantities (such as the median or geometric mean edge length, Maschberger and Clarke 2011; Olczak et al. 2011) which are less sensitive to the maximum edge length.

Finally it should be noted that MST-based methods can be applied to comparing the spatial distributions of stars as a function of age (as proxied by their possession of circumstellar disc diagnostics; see Ercolano et al. 2011).

3.1.3 Characterising the IMF

A widely used approach to describing the stellar mass function is to construct a log-log histogram such that—for a power-law IMF—the slope of the histogram gives the power-law index of the IMF. This is however problematical in several ways, as pointed out by Maíz Apellániz and Úbeda (2005). Firstly the derived slope is often sensitive to the binning. Secondly, Poissonian errorbars are largest in a log-log plot in the case of bins containing few objects (i.e. generally at high masses) and such errorbars are moreover asymmetric. This means that owing to Poisson noise, bins at high mass can frequently be sparsely populated. This introduces a bias which results in derived power laws being systematically too steep. The problem can be addressed by adopting bin sizes such that bins all contain the same number of objects. However this inevitably leads to large bin widths at the sparsely populated (high-mass) end of the IMF and thus reduces discrimination in this regime.

It is therefore preferable to use non-parametric tests (such as the Kolmogorov-Smirnov [KS] test) to test the consistency between observational data and a range of hypothesised functional forms. However, it needs to be borne in mind that the KS test is notoriously insensitive to deviations between distributions that occur near the extremes of the cumulative distribution: this is particularly problematical if one is trying to test, for example, whether data is consistent with an unbounded power-law or whether it requires a form that is truncated at high masses (this being

an area of considerable debate: see discussion in Sect. 7.2.1 of Chap. 7). This can be remedied by applying a stabilising transformation to the variables (such that the test is uniformly sensitive at all centile values; see Maschberger and Kroupa 2009).

3.2 Simulation Results: Bonnell et al. (2008) as a Case Study

In what follows we term as 'vanilla' calculations all those that incorporate the minimum subset of physics that is required to produce a somewhat realistic star-forming complex. Such calculations incorporate gravity (obviously!), a supersonic velocity field and thermal properties prescribed according to a barotropic equation of state (see Masunaga and Inutsuka 2000). In order to mimic 'turbulent' velocity fields, a common expedient is to start with an unstructured cloud and then to impose a divergence-free random Gaussian velocity field with a power spectrum [$P(k) \propto k^{-4}$] that is designed to reproduce the Larson size-linewidth relations (Larson 1981; see Sect. 1.4 of Chap. 1). We will start with the simplest case of a one-off injection of 'turbulent' kinetic energy and will contrast this in the following chapter with the case of continually driven turbulence or cases where the turbulence is 'settled' prior to the switch-on of gravity.

There is now a large body of such 'vanilla' calculations, following the pioneering simulations of Bate et al. (2002a). These vary greatly in scale and numerical resolution and range from relatively cheap calculations (such as those of Delgado-Donate et al. 2004; Goodwin et al. 2004a, b) where the small cloud masses permit multiple realisations of a given parameter set, to very expensive 'one-off' calculations which push the limits either in scale (e.g. Bonnell et al. 2008) or in resolution (e.g. Bate 2009, 2012). Naturally, the introduction of additional physical effects involves sacrifices in terms of scale and/or resolution.

From the point of view of simulating cluster formation, perhaps the most instructive are the largest scale simulations since they permit the treatment of an entire complex of clusters and can trace the history of their hierarchical assembly. Accordingly we start with a discussion of the largest scale star formation simulation conducted to date, i.e. that of Bonnell et al. (2008) which models a cloud of 10^4 $M_\odot$. At the end of the simulation (at an age of 0.5 Myr) around 1500 $M_\odot$ of gas has been converted into stars (i.e. sink particles) and these are distributed in a number of 'clusters' comprising hundreds of stars as well as a distributed population.

The initial configuration of the simulation is a cylinder of radius 3 pc and length 10 pc with a mild axial density gradient which ensures that—following introduction of the initial injection of turbulent energy—the cloud is overall marginally bound (being mildly bound at one end and mildly unbound at the other).

The evolution follows a sequence that is characteristic of all similar calculations: supersonic turbulence creates a web of shocked layers of compressed gas which break up under the action of self-gravity to create a network of dense filaments (note that this feature is broadly consistent with the widespread observations of filaments in *Herschel* observations of molecular clouds (André et al. 2010; Juvela

et al. 2012) although the simulations do not reproduce the invariant filament width that has has been reported in observations (Arzoumanian et al. 2011). In the simulations, small-scale inhomogeneities in the filaments are amplified by self-gravity and lead to fragmentation. The minimum spacing of such fragments is set by the characteristic (Jeans) length scale for collapse (see Eq. 1.2) for which the sound crossing and free-fall timescales along the length of the filament are similar. Stars (i.e. sinks) that form in a filament then follow large-scale self-gravitating flows along the filament and are thus transported towards the dense regions formed where filaments intersect (this itself also being a location of further fragmentation and star formation). It is worth noting at this stage that fragmentation often produces few body clusters and it is these (rather than single stars) that are conveyed along filaments.

This sequence of events leads to the formation of clusters via a bottom-up (hierarchical) process as demonstrated by the analysis of merger trees based on MST cluster identification (Maschberger et al. 2010). The ongoing merger sequence causes evolution of the Cartwrigth Q parameter which is low ('fractal') during the stage that (mini-)clusters are scattered along filaments but rises once mergers form a dominant centrally concentrated cluster. It should be stressed that these are not 'dry' (gas-free mergers) and that the gas (which remains the dominant mass component on large scales throughout the duration of the simulations, $\sim$0.5 Myr) plays an important role in channeling clusters together and facilitating the merger process.

If one looks at the properties of the clusters formed after 0.5 Myr (bearing in mind that the definition of a cluster depends on a particular choice of the 'cut-length' for the MST) one finds about 15 clusters containing more than 10 stars; obviously it is not sensible to define a formal cluster mass function from only 15 objects but it is clear that low-N clusters are more numerous and that the distribution is broadly compatible with the observed cluster mass function (where the fraction of clusters between N and $N + \mathrm{d}N$ scales as N^{-2}; Lada and Lada 2003). The most populous cluster in the simulations contains several hundred stars. These clusters are generally mildly aspherical (i.e. most frequently with projected axis ratios on the sky in the range of 1–2, though a few objects are at times more drastically aspherical). The cluster shape is sensitive to the history of mergers in the cluster, with highly aspherical shapes during ongoing mergers but with stellar two-body relaxation effects reducing the ellipticity between mergers. It is also found that these clusters are markedly mass segregated (especially the more populous clusters i.e. $N > 50$) at an age of 0.5 Myr; technically, this mass segregation is *not* primordial but is the result of rapid two-body relaxation within clusters that are assembled via mergers (see also McMillan et al. 2007; Allison et al. 2009, 2010). From an observational perspective, however, the system is so young that any observer would probably classify this situation as one of primordial mass segregation. It is worth noting that—as in the case of the ellipticity—the state of mass segregation changes during mergers: evidently while a merger is ongoing, there are two nuclei containing the most massive stars within a given cluster and this temporarily removes the mass segregation signature.

Before leaving this thumbnail portrait of cluster assembly in the Bonnell et al. (2008) simulation it is worth noting that the demographics of clustering within the simulation is quite sensitive to modest variations in the degree of gravitational

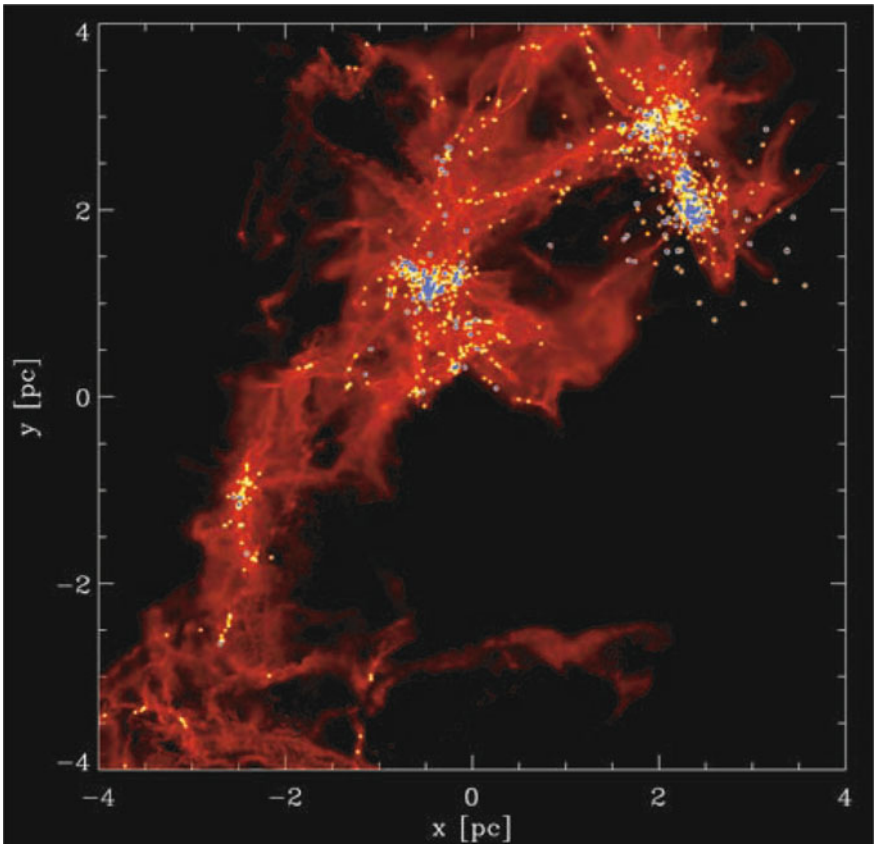

Fig. 3.3 The gas and stellar distribution in the simulation of Bonnell et al. (2008) at an age of ∼0.5 Myr. Note that the initial condition was cylindrical: the upper regions (where the populous clusters have formed) were initially mildly bound, whereas the lower half (where star formation is less intense) was initially mildly unbound. Figure from Bonnell et al. (2008)

boundedness in different regions of the simulation (see Fig. 3.3). As noted above, the mild density gradient along the axis of the initial gas cylinder means that the gas at one end is mildly unbound while it is mildly bound at the other end. Star formation proceeds more rapidly in the bound end of the cloud and the converging flows that develop along filaments lead to the formation of several populous clusters. At the unbound end, by contrast, much of the gas avoids significant compression and expands without forming stars: locally convergent flows do produce some stars even here but the large-scale flows are not conducive to significant merging and the star formation remains dispersed in rather small-N groupings.

We now proceed to a more general discussion of how various simulations of this 'vanilla' variety have contributed to our understanding of a range of issues in star and cluster formation.

3.3 The Relationship Between Gas, Cores and Stars in Simulations

Amongst the wealth of structures observed in molecular clouds there is a class of dense regions (identified in dust emission or absorption or else in molecular lines; see Chap. 1, Sect. 1.2) that are termed 'cores'. These are characterised by low internal velocity dispersions (comparable with the sound speed) and contain around a Jeans mass of gas. Such cores are widely regarded as being stellar progenitors and it is often claimed that the stellar mass function (IMF) is simply inherited from the core mass function (CMF, Motte et al. 1998; Johnstone and Bally 2006). We have already discussed 'the perils of clumpfind' (Pineda et al. 2009) and the difficulty in unambiguously identifying cores in observational data and this introduces some uncertainty about the reliability of observed CMFs. Nevertheless, from an observational perspective, comparison between the CMF and IMF is the only way to test the hypothesis that cores can be mapped directly onto resulting stars. Such a comparison has been claimed to indicate a systematic offset in logarithmic mass between the CMF and IMF (Lada et al. 2008), which can be interpreted as a universal 'efficiency' factor as cores turn into stars (see Goodwin et al. 2008 for an analysis of how this mapping is affected by the formation of multiple stars).

In the case of simulations, one has the luxury of being able to trace the fates of individual gas particles and of determining whether cores indeed turn directly into stars (bearing in mind the caveat that of course this does not necessarily indicate that the same evolutionary sequence is followed in reality!). Smith et al. (2009) identified gas cores in the simulations as local potential wells and showed that, in the simulations, the CMF and resulting IMF were indeed of similar functional form. However, they found that this situation represents a rather weak association between the masses of individual cores and the masses of the stars they produced—there is no more than a general tendency for more massive stars to form from more massive cores as the correspondence is blurred by the effect of subsequent accretion. Bonnell et al. (2004) also traced the assembly history of individual stars and showed that whereas low-mass stars form from rather local collapse, higher mass stars have mass contributions from a much larger volume. This is because stars that end up with high mass in the simulations are those that arrive early in cluster cores and are then able to accrete vigorously from a mass reservoir that is fed by material flowing in along filaments.

3.4 The Origin of the Stellar IMF in 'Vanilla' Calculations

Simulations of this kind routinely produce stellar (i.e. sink) IMFs which can be represented as a broken power-law—at high masses (above the so-called 'knee' of the IMF), the fraction of stars with masses between m and $m + \mathrm{d}m$ is $\propto m^{-\alpha}\mathrm{d}m$ where $\alpha \sim 2$ (comparable with the observed 'Salpeter' value of 2.35). Below the

knee, the mass function is flatter (i.e. with $\alpha \sim 1.5$) and this functional form imparts the distribution with a 'characteristic' mass that is similar to the knee mass. Early simulations were conspicuously successful in creating an IMF that is well matched to the observed form (Bate et al. 2002a, b, 2003) with knee values of around a solar mass. This is however entirely fortuitous (with regard to the value of the knee) since in the case of an isothermal equation of state (as employed in all these simple 'vanilla' calculations) the knee value is simply related to the mean Jeans mass in the cloud at the onset of the simulation (Bonnell et al. 2006). A simple dependence on mean Jeans mass (and an insensitivity to the Mach number of the turbulence) is in fact in contrast to the conclusions based on studies of non-self-gravitating turbulence (Padoan and Nordlund 2002; Hennebelle and Chabrier 2008) in which an IMF is constructed by constructing nominally Jeans unstable peaks in the turbulent density field. In this case, the mean stellar mass decreases at large Mach number, since this increases the density of shocked layers and thus lowers the nominal Jeans mass associated with such layers. It is interesting that whereas the self-gravitating simulations also produce denser structures at high Mach number, this does not translate into lower mass stars as would be suggested by application of this simple Jeans criterion. The reason for this discrepancy is probably the inapplicability of a simple (density-based) Jeans criterion in slab geometry: compression in such geometry—which changes neither the lateral sound crossing time nor lateral free-fall time—has little effect on the Jeans mass (see Lubow and Pringle 1993; Whitworth et al. 1994; Bonnell et al. 2004).

Although there is some interest in studying the differences between the IMFs inferred from non-self-gravitating density fields and those produced in simulations which allow collapse and subsequent accretion, it should not detract from a much more fundamental problem with all isothermal calculations. It is strongly undesirable to have a situation where the 'knee' of the IMF can be simply shifted around by a change in mean cloud density and temperature (see Fig. 3.4). This is because the observed IMF appears to be remarkably invariant in all well studied regions (see Bastian et al. 2010 for a recent review of this issue) whereas star-forming clouds

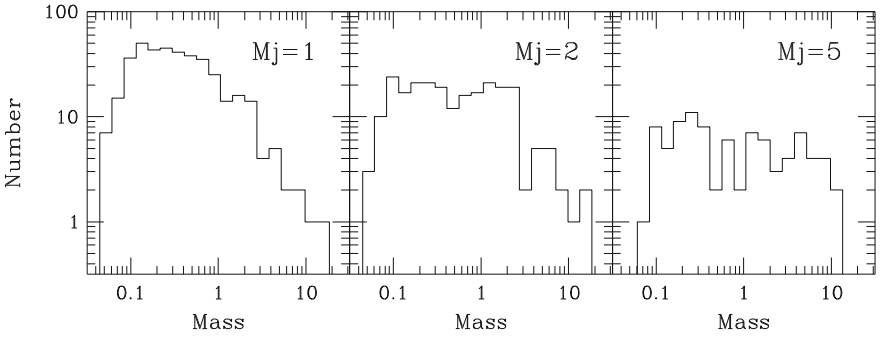

Fig. 3.4 Illustration of the IMFs produced in three different isothermal calculations in which the mean Jeans mass at the onset of the simulation is 1, 2 and 5 $M_\odot$ (*left* to *right* respectively). The 'knee' of the IMF then simply tracks the initial Jeans mass. Figure from Bonnell et al. (2006)

have a range of densities and temperatures which should—in this picture—cause corresponding variations in the IMF. It is however found that the situation may be remedied by using a rather modest departure from an isothermal equation of state. Larson (2005) proposed a barotropic equation of state in which the temperature falls mildly with increasing density ($T \propto \rho^{-0.25}$) in the regime dominated by line cooling (at number densities less than $10^6\,\mathrm{cm}^{-3}$) but rises mildly with density ($T \propto \rho^{0.1}$) at higher density where dust cooling becomes important (see also Whitworth et al. 1998 for a similar proposal that the conditions associated with the onset of dust cooling imprint a characteristic Jeans mass on the IMF). Certainly, Bonnell et al. (2006) found that this modest revision of the equation of state had a remarkably stabilising effect on the IMF produced in simulations. Whereas in previous isothermal simulations, the IMF 'knee' had simply followed variations in the initial cloud Jeans mass, it was found that the modified equation of state produced similar IMFs for a range of cloud initial conditions. These authors argued that the IMF is imprinted at this mass scale because such an equation of state implies that the Jeans mass changes from being respectively more (less) density dependent than the free-fall time for densities below (above) this threshold. At higher density, the Jeans mass is less responsive to density changes on the free-fall time and this tends to suppress further fragmentation. Moreover, Larson (2005) argued that the relevant equation of state should not be very sensitive to the metallicity either, so that this adjustment might provide a good route to producing a near universal IMF. The recent hydrodynamic simulations of Dopcke et al. (2013) confirm that the metallicity dependence of the effect of dust cooling on the IMF is indeed rather mild, even down to extremely low ($<10^{-4}\mathrm{Z}_\odot$) metallicities.

Whatever the details of the cooling physics invoked, it is encouraging that physically motivated modifications of the thermal physics can indeed stabilise the IMF. It should however be stressed that this is only one of the currently discussed ways in which 'additional physics' can achieve this stabilisation and we discuss other ideas (such as those relating this stabilisation to radiative feedback) in the following chapter.

Finally, we turn to the upper power-law of the IMF in simulations, i.e. in the regime above the 'knee'. Here the -2 power-law is generally ascribed to the role of Bondi-Hoyle accretion along the lines of the analysis first proposed by Zinnecker (1982). Such accretion gives rise to an accretion rate that scales quadratically with stellar mass, and, for a given initial mass, $M_{\rm in}$, one can write an expression for the stellar mass at time t. One can then map a given range of initial masses $\mathrm{d}M_{\rm in}$ into the corresponding range of masses $\mathrm{d}M$ at time t, which yields the relationship $\mathrm{d}M_{\rm in} = M_{\rm in}^2\,\mathrm{d}M/M^2$. This then demonstrates that if one starts with a given small range of initial masses, these are transformed by accretion into a power-law probability density function for stellar mass with slope -2. Bonnell et al. (2001) examined this picture for the build-up of stellar mass through idealised simulations which placed stellar sinks in smooth collapsing parent gas distributions; they argued that, while the stars are more or less co-moving with the collapsing gas, the accretion cross-section associated with Bondi-Hoyle accretion (which scales as the relative star-gas velocity raised to the power of -4) is unphysically large and that instead the relevant cross-section is the smaller tidal radius: they showed that in this case the IMF slope should

scale as mass to the power of −1.5 and that this is well matched to the simulation results at low mass. However, once stars dominate the potential in the core of the cloud they form a virialised sub-system in which stellar velocity directions are randomised with respect to radially inflowing gas. The increased random velocity then reduces the Bondi-Hoyle accretion cross-section to less than the tidal limit; hence Bondi-Hoyle accretion becomes the dominant process, thus explaining the power-law tail of the mass function with index −2.

It is not clear how much this explanation based on 'toy' models applies to the large range of subsequent turbulent fragmentation simulations which all show a similar IMF morphology (i.e. slope changing from ~ -1.5 to ~ -2 at an IMF 'knee'). At first sight, these simulations—such as the Bonnell et al. (2008) simulation described in detail above—bear little resemblance to the 'toy' model of a smooth radially collapsing gaseous background, since the turbulence generates a complex velocity and density field in the gas. Nevertheless, there may be more resemblance between the two situations than is visually apparent: Offner et al. (2009) demonstrated that when stars are formed in turbulent calculations their initial velocities with respect to the local gas is indeed low. On the other hand Kruijssen et al. (2012) showed that once clusters start to form via the hierarchical assembly process described above they form sub-systems which are in rough virial equilibrium and for which the increased relative velocity between stars and gas would make Bondi-Hoyle accretion a relevant process. This is consistent with the result mentioned above in which low-mass stars form from accretion of rather localised gas whereas more massive stars can attain a large fraction of their mass via accretion in cluster cores. Although this picture might still have some relevance to how the simulations build up stellar mass (and we emphasise that this is of course not the same as demonstrating its relevance to stellar mass acquisition in *real* systems), it should be noted that simulations apparently do *not* obey the quadratic relationship between stellar mass and accretion rate that under-pins the Bondi-Hoyle argument (Maschberger et al. 2014).

Before we leave such 'vanilla' calculations, it is worth dwelling further on the result that we have just noted, i.e. that the stellar motions within forming clusters appear to be in rough virial equilibrium with the potential produced by the stars alone and thus that the clusters within the simulations are internally gas-poor. This result does not appear to be a numerical issue with sink particle accretion inasmuch as the rapid accretion of gas within the region of the clusters dominated by the stars is insensitive to sink particle radius and resolution (Kruijssen et al. 2012) and also to numerical method (i.e. a similar result is found in the AMR based simulations of Girichidis et al. 2012). This result—if true also in the case of real protoclusters—would have profound consequences for the issue of cluster survival which we will discuss further in Chap. 6: it is often assumed that many star clusters become unbound (so-called cluster 'infant mortality') when gas—which was previously assumed to be the dominant mass component within embedded stellar clusters—was expelled. If in fact the clusters are already gas-poor on the scale of the stars (i.e. if the mass reservoir for further star formation is mainly located outside the stellar cluster) then gas-loss becomes irrelevant for star cluster survival.

3.5 Summary

We have surveyed the range of statistical descriptors that are used in the analysis of both observational data and the output of simulations, considering such issues as the spatial distribution of gas and stars, the stellar IMF, clustering and stellar mass segregation. We have then proceeded to a thumb-nail portrait of the largest scale simulation of cluster formation yet conducted—that of Bonnell et al. (2008) which models a cloud of mass $10^4\,M_\odot$ which forms around 15 star clusters over a timescale of $\sim$0.5 Myr. Although this simulation is considerably less sophisticated in terms of the physical processes modelled than are some of the simulations described in Chap. 4, it has nevertheless introduced some of the generic properties of cluster formation simulations. In particular we have drawn attention to the hierarchical nature of cluster assembly: the basic unit of cluster assembly on all scales is the small N ($<$10) cluster and large-scale clustering proceeds through a process of successive gas-mediated cluster mergers.

References

Allison, R. J., Goodwin, S. P., Parker, R. J., Portegies Zwart, S. F., & de Grijs, R. 2010, MNRAS, 407, 1098
Allison, R. J., Goodwin, S. P., Parker, R. J., et al. 2009, MNRAS, 395, 1449
André, P., Men'shchikov, A., Bontemps, S., et al. 2010, A&A, 518, L102
Arzoumanian, D., André, P., Didelon, P., et al. 2011, A&A, 529, L6
Bastian, N., Covey, K. R., & Meyer, M. R. 2010, ARA&A, 48, 339
Bate, M. R. 2009, MNRAS, 392, 590
Bate, M. R. 2012, MNRAS, 419, 3115
Bate, M. R., Bonnell, I. A., & Bromm, V. 2002a, MNRAS, 332, L65
Bate, M. R., Bonnell, I. A., & Bromm, V. 2002b, MNRAS, 336, 705
Bate, M. R., Bonnell, I. A., & Bromm, V. 2003, MNRAS, 339, 577
Bate, M. R., Clarke, C. J., & McCaughrean, M. J. 1998, MNRAS, 297, 1163
Blitz, L. & Stark, A. A. 1986, ApJ, 300, L89
Boldyrev, S. 2002, ApJ, 569, 841
Bonnell, I. A., Bate, M. R., & Vine, S. G. 2003, MNRAS, 343, 413
Bonnell, I. A., Clark, P., & Bate, M. R. 2008, MNRAS, 389, 1556
Bonnell, I. A., Clarke, C. J., & Bate, M. R. 2006, MNRAS, 368, 1296
Bonnell, I. A., Clarke, C. J., Bate, M. R., & Pringle, J. E. 2001, MNRAS, 324, 573
Bonnell, I. A., Vine, S. G., & Bate, M. R. 2004, MNRAS, 349, 735
Cartwright, A. & Whitworth, A. P. 2004, MNRAS, 348, 589
Delgado-Donate, E. J., Clarke, C. J., Bate, M. R., & Hodgkin, S. T. 2004, MNRAS, 351, 617
Dopcke, G., Glover, S. C. O., Clark, P. C., & Klessen, R. S. 2013, ApJ, 766, 103
Ercolano, B., Bastian, N., Spezzi, L., & Owen, J. 2011, MNRAS, 416, 439
Girichidis, P., Federrath, C., Banerjee, R., & Klessen, R. S. 2012, MNRAS, 420, 613
Goodwin, S. P., Nutter, D., Kroupa, P., Ward-Thompson, D., & Whitworth, A. P. 2008,A&A, 477, 823
Goodwin, S. P., Whitworth, A. P., & Ward-Thompson, D. 2004a, A&A, 414, 633
Goodwin, S. P., Whitworth, A. P., & Ward-Thompson, D. 2004b, A&A, 423, 169
Hennebelle, P. & Chabrier, G. 2008, ApJ, 684, 395

Johnstone, D. & Bally, J. 2006, ApJ, 653, 383
Johnstone, D., Wilson, C. D., Moriarty-Schieven, G., et al. 2000, ApJ, 545, 327
Juvela, M., Ristorcelli, I., Pagani, L., et al. 2012, A&A, 541, A12
Klessen, R. S. & Burkert, A. 2000, ApJS, 128, 287
Kruijssen, J. M. D., Maschberger, T., Moeckel, N., et al. 2012, MNRAS, 419, 841
Lada, C. J. & Lada, E. A. 2003, ARA&A, 41, 57
Lada, C. J., Muench, A. A., Rathborne, J., Alves, J. F., & Lombardi, M. 2008, ApJ, 672, 410
Larson, R. B. 1981, MNRAS, 194, 809
Larson, R. B. 1995, MNRAS, 272, 213
Larson, R. B. 2005, MNRAS, 359, 211
Lubow, S. H. & Pringle, J. E. 1993, MNRAS, 263, 701
Maíz Apellániz, J. & Úbeda, L. 2005, ApJ, 629, 873
Maschberger, T., Bonnell, I. A., Clarke, C. J., & Moraux, E. 2014, MNRAS, 439, 234
Maschberger, T. & Clarke, C. J. 2011, MNRAS, 416, 541
Maschberger, T., Clarke, C. J., Bonnell, I. A., & Kroupa, P. 2010, MNRAS, 404, 1061
Maschberger, T. & Kroupa, P. 2009, MNRAS, 395, 931
Masunaga, H. & Inutsuka, S.-I. 2000, ApJ, 531, 350
McMillan, S. L. W., Vesperini, E., & Portegies Zwart, S. F. 2007, ApJ, 655, L45
Men'shchikov, A., André, P., Didelon, P., et al. 2010, A&A, 518, L103
Moeckel, N. & Bonnell, I. A. 2009, MNRAS, 396, 1864
Motte, F., Andre, P., & Neri, R. 1998, A&A, 336, 150
Offner, S. S. R., Hansen, C. E., & Krumholz, M. R. 2009, ApJ, 704, L124
Olczak, C., Spurzem, R., & Henning, T. 2011, A&A, 532, 119
Padoan, P. & Nordlund, Å. 2002, ApJ, 576, 870
Padoan, P., Boldyrev, S., Langer, W., & Nordlund, Å. 2003, ApJ, 583, 308
Padoan, P., Cambrésy, L., Juvela, M., et al. 2006, ApJ, 649, 807
Parker, R. J., Bouvier, J., Goodwin, S. P., et al. 2011, MNRAS, 412, 2489
Peretto, N., André, P., Könyves, V., et al. 2012, A&A, 541, 63
Pineda, J. E., Rosolowsky, E. W., & Goodman, A. A. 2009, ApJ, 699, L134
Rosolowsky, E. W., Pineda, J. E., Kauffmann, J., & Goodman, A. A. 2008, ApJ, 679, 1338
Schmeja, S., Kumar, M. S. N., & Ferreira, B. 2008, MNRAS, 389, 1209
Schneider, N., Csengeri, T., Hennemann, M., et al. 2012, A&A, 540, L11
Simon, M. 1997, ApJ, 482, L81
Smith, R. J., Clark, P. C., & Bonnell, I. A. 2008, MNRAS, 391, 1091
Smith, R. J., Clark, P. C., & Bonnell, I. A. 2009, MNRAS, 396, 830
Whitworth, A. P., Bhattal, A. S., Chapman, S. J., Disney, M. J., & Turner, J. A. 1994, A&A, 290, 421
Whitworth, A. P., Boffin, H. M. J., & Francis, N. 1998, MNRAS, 299, 554
Williams, J. P., de Geus, E. J., & Blitz, L. 1994, ApJ, 428, 693
Zinnecker, H. 1982, Annals of the New York Academy of Sciences, 395, 226